Soft Matter

Intermediate crystalline structures of colloids in shape space

Journal:	*Soft Matter*
Manuscript ID	SM-ART-08-2018-001573
Article Type:	Paper
Date Submitted by the Author:	01-Aug-2018
Complete List of Authors:	Klotsa, Daphne; University of North Carolina at Chapel Hill, Applied Physical Sciences Chen, Elizabeth; Harvard University, Engel, Michael; University of Erlangen-Nürnberg, Glotzer, Sharon; University of Michigan, Chemical Engineering

Intermediate crystalline structures of colloids in shape space

Daphne Klotsa,[1,2,*] Elizabeth R. Chen,[1,3] Michael Engel,[1,4] and Sharon C. Glotzer[1,5,†]

[1] *Department of Chemical Engineering, University of Michigan, Ann Arbor, Michigan, 48109, USA*
[2] *Department of Applied Physical Sciences, University of North Carolina, Chapel Hill, North Carolina 27599, United States*
[3] *Harvard University School of Engineering and Applied Sciences, Cambridge MA, USA*
[4] *Institute for Multiscale Simulation, Friedrich-Alexander University Erlangen-Nürnberg, 91052 Erlangen, Germany*
[5] *Department of Materials Science and Engineering, University of Michigan, Ann Arbor, Michigan, 48109, USA*

(Dated: August 1, 2018)

We computationally study the thermodynamic assembly of more than 40,000 hard, convex polyhedra belonging to three families of shapes associated with the triangle groups 323, 423, and 523. Each family is defined by vertex and/or edge truncation of symmetric polyhedra with equal edge length, producing shapes for which the majority are intermediates of more symmetric polyhedra found among the Platonic, Archimedean, and Catalan solids. In addition to the complex crystals cI16 lithium, BC8 silicon, γ-brass, β-manganese, and a dodecagonal quasicrystal, we find that most intermediate shapes assemble distorted variants of four basic cubic crystals: face-centered cubic, body-centered cubic, simple cubic, and diamond. To quantify the degree of distortion, we developed an algorithm that extracts lattice vectors from particle positions and then evaluates closeness to the four reference cubic crystals. This analysis allows us to group together in shape space related intermediate structures that would otherwise be placed in different lattice systems had we followed the lattice systems' strict definitions for angles and lengths of lattice vectors. The resulting landscapes show, as a function of shape, regions where ordered structures assemble, what is assembled and at what density, locations of transitions between regions of ordered structures, and regions of disorder. Our results provide a guide to self-assembling a host of related colloidal crystals through systematic design, through careful tweaking of particle shape.

I. INTRODUCTION

With the growing interest in assembling colloidal crystals from nanometer- to micron-sized particles for a host of applications, it is important to understand how particle attributes relate to the thermodynamically stabilized crystals into which the particles assemble [1–10]. Computer simulations now easily allow studies of families of continuously related shapes, permitting the discovery of trends in crystal structure as particle shape is varied smoothly and systematically. In one-parameter families of shapes, the shape is varied between two ends of commonly known symmetric shapes. Examples include bowls where the thickness of the bowl is varied [11], superballs that interpolate between a cube and an octahedron via a sphere [6, 12, 13], polyhedra interpolating between a tetrahedron and an octahedron [4], and polyhedra interpolating between a cube and an octahedron [7]. All these works predict crystal structures that change as a function of particle shape. Unlike atoms, colloidal particles do not obey charge quantization, and thus intermediate structures are not only possible, but expected. Intermediate shapes between the two ends of the interpolation between regular shapes assemble structures that have been reported as distorted versions of basic crystals [7, 12, 13]. It is these distorted structures we focus on here. We argue that understanding distorted – or, as we shall call them, *intermediate* – structures is important because i) they are abundant, as we will show; ii) they may be relevant for experiments, as experimentally synthesized shapes may be intermediate shapes; iii) they may have interesting macroscopic properties in their own right, opening up the parameter space for materials; iv) they may be useful for gaining insight into structural transitions as a function of shape; and v) they can be useful for designing glass-forming shapes that do not assemble any ordered structure.

In this paper, we computationally study the thermodynamic assembly of tens of thousands of hard, symmetric, convex polyhedra that belong to three families of continuously modified shapes, and quantify the degree of distortion of colloidal crystal structures assembled by intermediate shapes by introducing an algorithm that extracts lattice vectors from particle positions and evaluates the similarity of the intermediate structure to four reference crystals: face-centered cubic (FCC), body-centered cubic (BCC), simple cubic (SC), and diamond (DIA). This analysis allows us to group together in shape space related structures that would otherwise be placed in different lattice systems (triclinic, monoclinic, orthorhombic, tetragonal, hexagonal, cubic) had we followed the lattice systems' strict definitions for angles and lengths of lattice vectors. Our results are presented as "assembly landscapes" – surfaces of the minimum density for self-assembly vs. shape parameters – that reveal regions in shape space where ordered structures assemble, locations of transitions between ordered structures, and regions of

* dklotsa@email.unc.edu
† sglotzer@umich.edu

disorder. We find that the minimum assembly density systematically increases towards the edges of regions of order, indicating a tendency towards decreasing thermodynamic stability of the ordered phase relative to that of the disordered fluid. In addition to distorted crystal structures, we find complex crystal structures in isolated regions of shape space. These structures include cI16 lithium (Li), γ-brass, β-manganese (Mn), a dodecagonal quasicrystal (QC), and, here reported for the first time, BC8 silicon (Si). We conclude by comparing our assembly landscapes to previously reported putative densest packing landscapes evaluated for the same three shape families [14].

II. MODEL AND METHODS

A. Shape families

We studied three families of shapes that have tetrahedral symmetry (triangle group 323), octahedral/cubic symmetry (triangle group 423), and icosahedral/dodecahedral symmetry (triangle group 523), as in [14], see Fig. 1a-c. Polyhedra are constructed by applying edge truncation and/or vertex truncation to all five Platonic solids defining three domains of two-parameter shape families with parameters $0 \leq a, c \leq 100$ (Fig. 1a-c). The most regular polyhedra are found in the four corners of each domain. For family 323 (Fig. 1a), clockwise from top left is the cube, octahedron, tetrahedron, and tetrahedron. For family 423 (Fig. 1b), clockwise from top left is the cube, octahedron, rhombic dodecahedron, and cuboctahedron. For the family 523 (Fig. 1c), clockwise from top left is the dodecahedron, icosahedron, rhombic triacontahedron, and icosidodecahedron. Some other regular polyhedra are found in the interior; these include the cuboctahedron (at $a = 50, c = 50$ in 323 family, Fig. 1a), truncated octahedron (at $25, 25$ in 523 family, Fig. 1c), and truncated icosahedron, also known as the buckyball (at $25, 0$ in 523 family, Fig. 1c).

B. Self-assembly simulations

We performed isochoric Monte-Carlo (MC) simulations in shape-fluctuating boxes as in [1, 4, 5]. Shapes were defined as hard particles with only steric interaction. Potential overlaps between polyhedra were identified through the Gilbert-Johnson-Keerthi algorithm [15] and discarded. Each simulation contained $N = 2000$ particles in a periodic box initiated from an equilibrated fluid phase at packing fraction (density) $\phi = 0.4$. Most of the simulations spontaneously crystallized at densities $0.5 \leq \phi \leq 0.64$ within 5×10^6 MC steps. If a simulation did not crystallize within this time limit, we extended the run for another 200×10^6 MC steps. If still no crystal was observed within the second time limit, the system was labeled "disordered." We initially ran four independent simulations with different initializations for each shape in a parameter grid of 21×21 (441 shapes per family). In regions of shape space where we observed many different crystal structures in close proximity, we refined the search grid further, *e.g.*, for the tetrahedral family, for $a, c \leq 34$, we refined to a grid of 101×101 (40,804 simulations).

C. Structure identification

Initial structure identification was performed using bond orientational order diagrams (BODs). BODs are histograms of the directions of bonds connecting a particle to its nearest neighbors projected onto the surface of a unit sphere [16, 17]. Clear peaks indicate a well-formed crystal, and structurally distinct crystals yield different BODs. Disordered systems have isotropic BODs with no peaks. By construction, most of the shapes investigated here are intermediates between more regular polyhedra that define the boundaries (corners) of our shape space. Assemblies have been reported previously for these regular (corner) shapes [1, 4, 5, 18] and for a one-parameter 432 subfamily [7], and those results are confirmed here. For the intermediate shapes in our families, the BODs frequently appeared as distorted variants of the high-symmetry patterns that we typically observe for the regular shapes. We therefore require a more sophisticated method to quantify the distortion (shear) of the crystal unit cells.

D. Similarity to reference crystal structures

We assert that many of the crystals assembled here with distorted BODs are more usefully viewed as distorted/sheared versions of cubic reference crystal structures, *i.e.* intermediates. To analyze this relationship, we extract basis vectors from particle simulation data that assemble periodic structures and then quantify how close the data are to reference crystals: SC, BCC, FCC, and DIA [19].

1. Unit cell extraction

Starting from a set of N particle positions $\{\boldsymbol{r}_n\}$, we analyze the peak positions of the structure factor

$$S(\boldsymbol{q}) = \frac{1}{N}\left|\sum_{n=1}^{N} \exp(i\boldsymbol{q}\cdot\boldsymbol{r}_n)\right|^2$$

taking into account symmetry, extinction and interference effects. Given a reference crystal structure, we select a set of M diffraction peaks $\{(h_m k_m \ell_m)\}$ and search

for a basis in reciprocal space $\{\boldsymbol{b}_1, \boldsymbol{b}_2, \boldsymbol{b}_3\}$ that maximizes

$$\nu = \sum_{m=1}^{M} S(h_m \boldsymbol{b}_1 + k_m \boldsymbol{b}_2 + \ell_m \boldsymbol{b}_3).$$

Specifically, we use $M_{\rm SC} = 6$, $M_{\rm BCC} = 12$, $M_{\rm FCC} = 8$, $M_{\rm DIA} = 4$ diffraction peaks allowed by selection rules,

$$\begin{aligned}
\{(hk\ell)\}_{\rm SC} &= \{\langle 200\rangle\},\\
\{(hk\ell)\}_{\rm BCC} &= \{\langle 110\rangle\},\\
\{(hk\ell)\}_{\rm FCC} &= \{\langle 111\rangle\},\\
\{(hk\ell)\}^{+}_{\rm DIA} &= \{\langle 111\rangle : hk\ell = +1\},\\
\{(hk\ell)\}^{-}_{\rm DIA} &= \{\langle 111\rangle : hk\ell = -1\}.
\end{aligned}$$

Note that the choices $\{(hk\ell)\}^{+}_{\rm DIA}$ and $\{(hk\ell)\}^{-}_{\rm DIA}$ lead to identical quantifications, but we list both for symmetry. In our algorithm, the search is performed by testing 10^6 random values for the reciprocal lattice basis. From each reciprocal lattice basis of a reference crystal structure, we obtain the corresponding lattice basis $\{\boldsymbol{\zeta}, \boldsymbol{\xi}, \boldsymbol{\varsigma}\}$ in real space.

2. Color map

We quantify how similar the obtained lattice bases are to those of the reference crystal structures. For this purpose, we measure orthogonality of vector angles,

$$\begin{aligned}
\lambda^{\rm angle}_{\rm point} &= \frac{\det\{\boldsymbol{\zeta}, \boldsymbol{\xi}, \boldsymbol{\varsigma}\}^{2/3}}{(\boldsymbol{\zeta}^2\boldsymbol{\xi}^2\boldsymbol{\varsigma}^2)^{1/3}},\\
\lambda^{\rm angle}_{\rm plane} &= \frac{\det\{\boldsymbol{\xi}\times\boldsymbol{\varsigma}, \boldsymbol{\varsigma}\times\boldsymbol{\zeta}, \boldsymbol{\zeta}\times\boldsymbol{\xi}\}^{2/3}}{((\boldsymbol{\xi}\times\boldsymbol{\varsigma})^2(\boldsymbol{\varsigma}\times\boldsymbol{\zeta})^2(\boldsymbol{\zeta}\times\boldsymbol{\xi})^2)^{1/3}},
\end{aligned}$$

and equality of vector lengths,

$$\begin{aligned}
\lambda^{\rm length}_{\rm point} &= \frac{(\boldsymbol{\zeta}^2\boldsymbol{\xi}^2\boldsymbol{\varsigma}^2)^{1/3}}{\frac{1}{3}(\boldsymbol{\zeta}^2+\boldsymbol{\xi}^2+\boldsymbol{\varsigma}^2)},\\
\lambda^{\rm length}_{\rm plane} &= \frac{((\boldsymbol{\xi}\times\boldsymbol{\varsigma})^2(\boldsymbol{\varsigma}\times\boldsymbol{\zeta})^2(\boldsymbol{\zeta}\times\boldsymbol{\xi})^2)^{1/3}}{\frac{1}{3}((\boldsymbol{\xi}\times\boldsymbol{\varsigma})^2+(\boldsymbol{\varsigma}\times\boldsymbol{\zeta})^2+(\boldsymbol{\zeta}\times\boldsymbol{\xi})^2)}
\end{aligned}$$

and combine them into

$$\begin{aligned}
\lambda^{\rm angle} &= \lambda^{\rm angle}_{\rm point}\lambda^{\rm angle}_{\rm plane},\\
\lambda^{\rm length} &= \lambda^{\rm length}_{\rm point}\lambda^{\rm length}_{\rm plane},\\
\lambda &= \lambda^{\rm angle}\lambda^{\rm length}.
\end{aligned}$$

Note that $\det\{\boldsymbol{\xi}\times\boldsymbol{\varsigma}, \boldsymbol{\varsigma}\times\boldsymbol{\zeta}, \boldsymbol{\zeta}\times\boldsymbol{\xi}\} = \det\{\boldsymbol{\zeta}, \boldsymbol{\xi}, \boldsymbol{\varsigma}\}^2$. Similarity to reference crystal structures is measured by

$$\begin{aligned}
\mu_{\rm SC}\{\boldsymbol{\zeta}, \boldsymbol{\xi}, \boldsymbol{\varsigma}\} &= \lambda\{\boldsymbol{\zeta}, \boldsymbol{\xi}, \boldsymbol{\varsigma}\},\\
\mu_{\rm BCC}\{\boldsymbol{\zeta}, \boldsymbol{\xi}, \boldsymbol{\varsigma}\} &= \lambda\{\boldsymbol{\xi}+\boldsymbol{\varsigma}-\boldsymbol{\zeta}, \boldsymbol{\varsigma}+\boldsymbol{\zeta}-\boldsymbol{\xi}, \boldsymbol{\zeta}+\boldsymbol{\xi}-\boldsymbol{\varsigma}\},\\
\mu_{\rm FCC}\{\boldsymbol{\zeta}, \boldsymbol{\xi}, \boldsymbol{\varsigma}\} &= \lambda\{\boldsymbol{\xi}+\boldsymbol{\varsigma}, \boldsymbol{\varsigma}+\boldsymbol{\zeta}, \boldsymbol{\zeta}+\boldsymbol{\xi}\},\\
\mu_{\rm DIA}\{\boldsymbol{\zeta}, \boldsymbol{\xi}, \boldsymbol{\varsigma}\} &= \lambda\{\boldsymbol{\xi}+\boldsymbol{\varsigma}, \boldsymbol{\varsigma}+\boldsymbol{\zeta}, \boldsymbol{\zeta}+\boldsymbol{\xi}\}.
\end{aligned}$$

We choose colors for the assembly landscapes and the previously reported putative densest packing landscapes using the following mapping onto the rgb color cube,

$$\begin{aligned}
\langle \text{red}, \text{green}, \text{blue}\rangle &= \langle (\mu_{\rm FCC})^p, (\mu_{\rm BCC})^p, (\mu_{\rm SC})^p\rangle,\\
\langle \text{red}, \text{green}, \text{blue}\rangle &= \langle (\mu^{\rm angle}_{\rm DIA})^q, 0, (\mu^{\rm length}_{\rm DIA})^q\rangle,
\end{aligned}$$

where we set $p = 4$ and $q = 2$ for contrast and

$$\begin{aligned}
\mu_4^{\rm angle}\{\boldsymbol{\zeta}, \boldsymbol{\xi}, \boldsymbol{\varsigma}\} &= \lambda^{\rm angle}\{\boldsymbol{\xi}+\boldsymbol{\varsigma}, \boldsymbol{\varsigma}+\boldsymbol{\zeta}, \boldsymbol{\zeta}+\boldsymbol{\xi}\},\\
\mu_4^{\rm length}\{\boldsymbol{\zeta}, \boldsymbol{\xi}, \boldsymbol{\varsigma}\} &= \lambda^{\rm length}\{\boldsymbol{\xi}+\boldsymbol{\varsigma}, \boldsymbol{\varsigma}+\boldsymbol{\zeta}, \boldsymbol{\zeta}+\boldsymbol{\xi}\}.
\end{aligned}$$

By the end of this analysis, we have reduced a high dimensional space to a single color that simultaneously tracks changes of magnitudes and/or angles of the lattice vectors for all our assembled structures with up to two particles in the primitive unit cell.

III. RESULTS

A. Assembly landscapes

We applied the algorithm and color map metric μ to the cubic structures FCC, BCC, SC, DIA and intermediate (distorted) versions of them. We separately identified crystals with unit cells with $n > 2$ and the quasicrystal using BODs. The disordered regions, also identified by their BODs, were not further characterized. We thus obtained diagrams showing assembly structure as a function of the two shape parameters for each family (Fig. 1g-i).

In the 323 family, the intermediate cubic structures occurred primarily along and on either side of the diagonal that connects the cube and octahedron, and at and around the truncated octahedron (near $a, c = 0, 20$ and near 25, 50), (Fig. 1g). Near the cube (at 100, 100), the algorithm identified intermediate structures related to SC. Moving along the diagonal (from the cube at the top right to the octahedron at the bottom left) there is a gradual but clear transition from SC to BCC to FCC, and then again to BCC near the corner at the octahedron (at 0,0). We also observe a region that assembled DIA including β-tin, which is distorted DIA. The structures with $n > 2$ form a region of cI16 Lithium (at 0,15) near the truncated octahedron, a region of the dodecagonal quasicrystal at and around the tetrahedron (at 0,100), as well as single points of BC8 silicon (at 30,10) and β-manganese (at 50,22).

In the 423 family, there are large regions of intermediate structures related to FCC and BCC, a smaller region of SC intermediate structures, and clear transitions between them (Fig. 1h). In contrast, the 523 family mostly assembled FCC intermediates. We observed a region of β-manganese and γ-brass for intermediate shapes near the left edge of the domain, near the dodecahedron. Regions of disorder were frequently found between structures that had different numbers n of particles in

their primitive unit cells, the exceptions being BC8 silicon ($n = 8$) adjacent to DIA ($n = 2$) and β-manganese ($n = 20$) adjacent to FCC ($n = 1$).

We also plotted the minimum assembly density as a function of the shape parameters (Fig. 1d-f), where we defined the minimum assembly density as the lowest packing fraction for which we observed crystal formation. In the 323 family, the minimum assembly density is lowest in the FCC region, $51-52\%$, higher for SC and BCC, $53-54\%$, and rapidly increased in all cases to greater than 60% as the disordered regions were approached from any structure (Fig. 1d). In the 423 family, the minimum assembly density was greater than 54% at the top left corner as well as along a vertical strip down in shape space, where SC and BCC intermediates formed. We observed a large region where FCC intermediates formed at minimum assembly density between $51-52\%$. Towards the bottom right corner of the 423 landscape, the minimum assembly density increased as FCC-intermediates transitioned to BCC-intermediates, and peaked at 62% towards the edge of the disordered region and for cI16 Lithium (Fig. 1e). In the 523 family, most shapes assembled FCC intermediates at minimum assembly densities $51-52\%$, while on the upper left edge of the domain, where γ-brass and β-manganese formed, the minimum assembly densities increased to $56-57\%$ (Fig. 1f).

As can be seen by comparing Fig. 1d-f with Fig. 1g-i, visual inspection of the minimum assembly density landscapes is all that is needed to identify regions of ordered structures and transitions between different structures, even without knowing the identity of the structures. Thus, structural signatures of the thermodynamic assemblies are reflected in the minimum assembly density, even though the two measurements are independent of one another.

B. Comparison to putative densest packing landscapes

We previously reported putative [20] densest packings for the three family of shapes studied here calculated through a combination of Monte Carlo simulations and analytic optimization [14]. Here, we applied the algorithm we used to identify intermediate structures in the assembly data to the putative densest packing data (Fig.1g-l) to make a direct comparison. The solid lines indicate regions of packings according to contacts calculated previously [14] and are shown here for reference. Of course, there is no *a priori* reason why the crystal that self-assembles at moderate densities should generally be the same as the mathematically optimized packing. The former arises from entropy maximization, while the latter arises from minimization of the Gibbs free energy in the limit of infinite pressure.

In comparing visually the assembly and packing landscapes for each family, we observe a general correspondence between assembly and densest packing for the simplest crystal structures. For the more complex structures, the putative densest packings generally differ from the observed assemblies. Of most relevance to this work is that those structures identified as intermediate in the assembly landscapes and labeled via the proposed metric to reflect their similarity to the basic cubic crystals, match the corresponding putative densest packings of the structures they are most similar to. This observation demonstrates a major strength of our metric, in that it reveals potential relationships between assemblies and packings that could be missed otherwise.

IV. DISCUSSION AND CONCLUSION

Through a large and comprehensive set of computer simulations requiring significant computational resources, we studied the thermodynamic assemblies of tens of thousands of polyhedra, most of which are intermediate shapes that occur through edge and/or vertex truncations of more symmetric polyhedra. We identified the cubic crystals SC, BCC, FCC, and DIA, as well as intermediate (distorted) versions of them, and more complex crystals, including cI16 lithium, BC8 silicon, γ-brass, β-manganese, and a dodecagonal quasicrystal. We presented an algorithm that easily identifies and accurately quantifies regions of intermediate crystal structures with reference to basic cubic crystals. The application of our algorithm to colloidal crystal assembly opens up new possibilities for designing materials properties that depend on targeting crystal structures having a given similarity to one of these reference structures.

As with previous works on packing, our structure and minimum assembly density landscapes can guide experiments and theory by serving as "phase diagrams for shape" – locating regions where crystals form, regions where crystals fail to form, and transitions between regions. For example, within regions that assemble crystals, our landscapes show how sensitive the assembly of a crystal in a given region is to small differences in particle shape within certain regions, and how insensitive assembly is to small differences in other regions where small shape changes merely change the similarity of the resulting crystal to a nearby reference crystal. Also, because experimentally synthesized shapes may differ from perfect polyhedra, such knowledge is useful to evaluate how accurately the shape must be synthesized to achieve successful assembly. For example, in the 323 family the region of shape space over which the cI16 lithium structure forms is much smaller than the region over which BCC forms (Fig. 1g), implying that to assemble the cI16 lithium structure shape synthesis must be more precise. The minimum assembly density landscapes provide guidance in selecting shapes for synthesis. For example, to assemble FCC it may be advisable to use the shape with the lowest minimum assembly density shown in the interior of the FCC region, 50% (in the 323 family, dark blue in Fig. 1d), than a shape at the edge of the FCC re-

gion where the minimum assembly density can be as high as 60%. Already studies have used our landscapes to, *e.g.*, quantify order-order transitions in shape space [21] and determine why shapes in the disordered regions fail to assemble crystals [22]. Furthermore, the correspondence we observe between two independent measures of a crystal assembled from a given shape – namely, our algorithm's structure identification and the minimum density for self assembly – indicates a connection between them that should be further investigated in future work.

ACKNOWLEDGMENTS

Acknowledgments. D.K. and E.R.C. contributed equally to this work. D.K. acknowledges a Marie Curie Postdoctoral International Outgoing Fellowship (IOF). E.R.C. acknowledges NSF grant MSPRF DMS-1204686. This work was partially supported by a Simons Investigator award from the Simons Foundation to S.C.G.

[1] Amir Haji-Akbari, Michael Engel, Aaron S. Keys, Xiaoyu Zheng, Rolfe G. Petschek, Peter Palffy-Muhoray, and Sharon C Glotzer, "Disordered, quasicrystalline and crystalline phases of densely packed tetrahedra," Nature **462**, 773–777 (2009).

[2] Umang Agarwal and Fernando A Escobedo, "Mesophase behaviour of polyhedral particles," Nature Materials **10**, 230–235 (2011).

[3] Carlos Avendaño and Fernando A Escobedo, "Phase behavior of rounded hard-squares," Soft Matter **8**, 4675 (2012).

[4] Pablo F. Damasceno, Michael Engel, and Sharon C. Glotzer, "Crystalline assemblies and densest packings of a family of truncated tetrahedra and the role of directional entropic forces," ACS Nano **6**, 609–614 (2012).

[5] Pablo F Damasceno, Michael Engel, and Sharon C Glotzer, "Predictive self-assembly of polyhedra into complex structures," Science **337**, 453–457 (2012).

[6] Ran Ni, Anjan Prasad Gantapara, Joost de Graaf, René van Roij, and Marjolein Dijkstra, "Phase diagram of colloidal hard superballs: from cubes via spheres to octahedra," Soft Matter **8**, 8826 (2012).

[7] Anjan P. Gantapara, Joost de Graaf, René van Roij, and Marjolein Dijkstra, "Phase diagram and structural diversity of a family of truncated cubes: Degenerate close-packed structures and vacancy-rich states," Physical Review Letters **111**, 015501 (2013).

[8] Mihir R. Khadilkar, Umang Agarwal, and Fernando A. Escobedo, "Phase behavior of binary mixtures of hard convex polyhedra," Soft Matter **9**, 11557 (2013).

[9] Mihir R Khadilkar and Fernando A Escobedo, "Heuristic rule for binary superlattice coassembly: Mixed plastic mesophases of hard polyhedral nanoparticles," Physical Review Letters **113**, 165504 (2014).

[10] Yina Geng, Greg van Anders, and Sharon C. Glotzer, "Predicting colloidal crystals from shapes via inverse design and machine learning," (2018), arXiv:1801.06219.

[11] Matthieu Marechal and Marjolein Dijkstra, "Phase behavior and structure of colloidal bowl-shaped particles: Simulations," Physical Review E **82**, 031405 (2010).

[12] Yugang Zhang, Fang Lu, Daniel van der Lelie, and Oleg Gang, "Continuous phase transformation in nanocube assemblies," Physical Review Letters **107**, 135701 (2011).

[13] Laura Rossi, Vishal Soni, Douglas J. Ashton, David J. Pine, Albert P. Philipse, Paul M. Chaikin, Marjolein Dijkstra, Stefano Sacanna, and William T. M. Irvine, "Shape-sensitive crystallization in colloidal superball fluids," Proceedings of the National Academy of Sciences **112**, 5286–5290 (2015).

[14] Elizabeth R Chen, Daphne Klotsa, Michael Engel, Pablo F. Damasceno, and Sharon C Glotzer, "Complexity in surfaces of densest packings for families of polyhedra," Physical Review X **4**, 011024 (2014).

[15] E.G. Gilbert, D.W. Johnson, and S.S. Keerthi, "A fast procedure for computing the distance between complex objects in three-dimensional space," IEEE Journal on Robotics and Automation **4**, 193–203 (1988).

[16] Paul J Steinhardt, David R Nelson, and Marco Ronchetti, "Bond-orientational order in liquids and glasses," Physical Review B **28**, 784–805 (1983).

[17] Wolfgang Lechner and Christoph Dellago, "Accurate determination of crystal structures based on averaged local bond order parameters," Journal of Chemical Physics **129**, 114707 (2008).

[18] Benjamin A Schultz, Pablo F Damasceno, Michael Engel, and Sharon C Glotzer, "Symmetry considerations for the targeted assembly of entropically stabilized colloidal crystals via Voronoi particles," ACS Nano **9**, 2336–2344 (2015).

[19] We do not distinguish between FCC and hexagonal-close packed (HCP) structures.

[20] We refer to these packings as "putative.

[21] Chrisy Xiyu Du, Greg van Anders, Richmond S Newman, and Sharon C Glotzer, "Shape-driven solidsolid transitions in colloids," Proceedings of the National Academy of Sciences **114**, E3892–E3899 (2017).

[22] E G Teich, G van Anders, and S.C.Glotzer, "Identity crisis in alchemical space drives the entropic colloidal glass transition," Nature Communications , under review (2018).

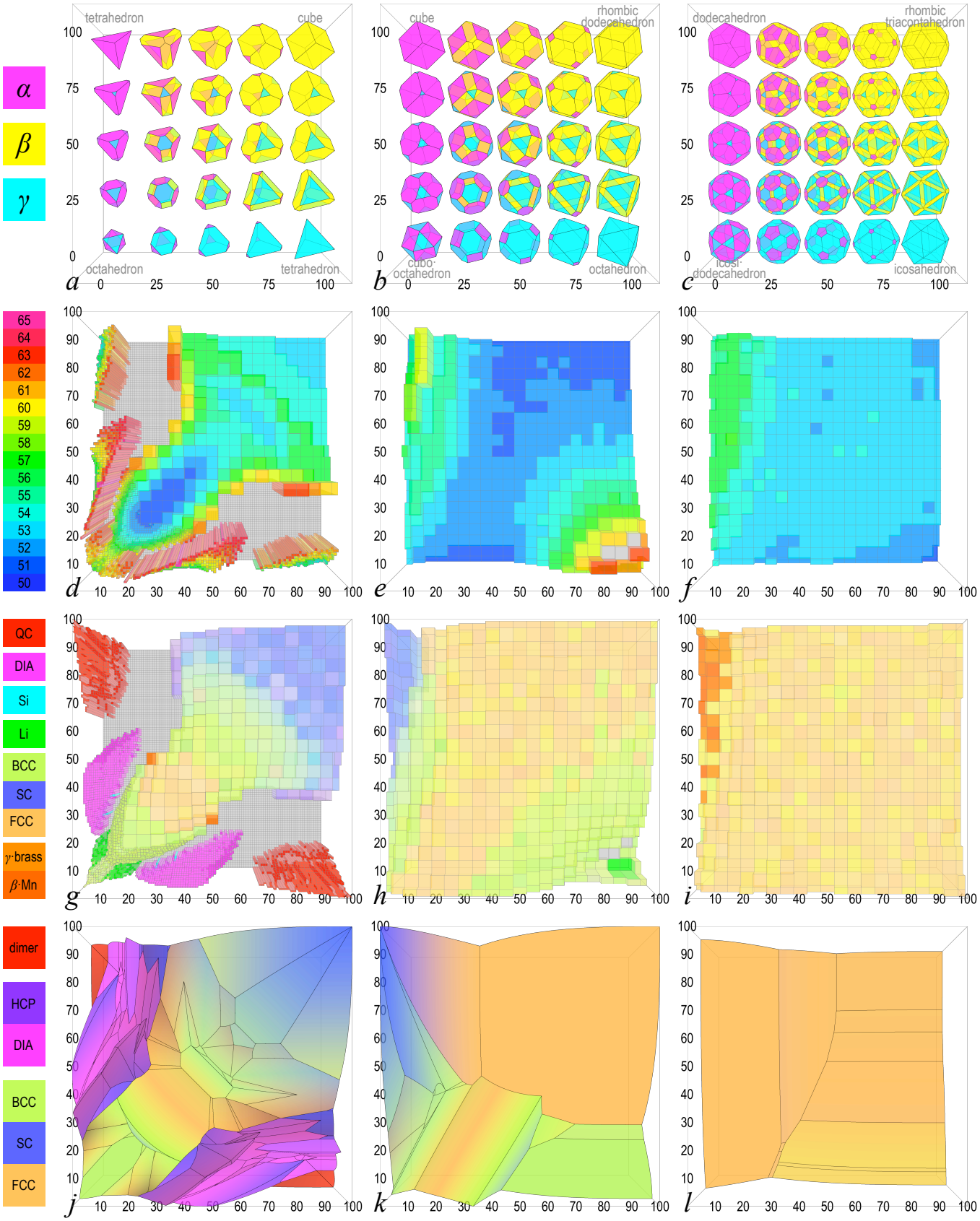

FIG. 1. Landscapes in shape space for minimum density for self-assembly, self-assembled crystal structure, and putative densest packings. Columns: shape family 323 (a,d,g,j), 423 (b,e,h,k), 523 (c,f,i,l). Rows: shapes (a-c), minimum assembly density (d-f), self-assembled structure (g-i), putative densest packing structure (j-l). In (d-i) height indicates minimum assembly density.